

5-2019

Characterizing Flame-resistant Polymers using Single-sided NMR

Anna Tsutsui

Follow this and additional works at: <https://scholarworks.wm.edu/honorsthesis>

 Part of the [Physical Chemistry Commons](#), and the [Polymer Chemistry Commons](#)

Recommended Citation

Tsutsui, Anna, "Characterizing Flame-resistant Polymers using Single-sided NMR" (2019). *Undergraduate Honors Theses*. Paper 1324.

<https://scholarworks.wm.edu/honorsthesis/1324>

This Honors Thesis is brought to you for free and open access by the Theses, Dissertations, & Master Projects at W&M ScholarWorks. It has been accepted for inclusion in Undergraduate Honors Theses by an authorized administrator of W&M ScholarWorks. For more information, please contact scholarworks@wm.edu.

Characterizing Flame-resistant Polymers using Single-sided NMR

by

Anna Tsutsui


Characterizing Flame-resistant Polymers using Single-sided NMR

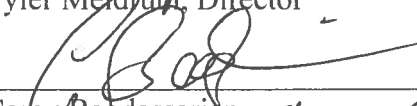
A thesis submitted in partial fulfillment of the requirement
for the degree of Bachelor of Science in Chemistry from
The College of William and Mary

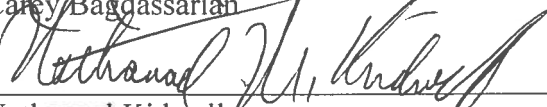
by

Anna Tsutsui

Accepted for HONORS
(Honors)


Tyler Meldrum, Director


Carey Bagdassarian


Nathanael Kidwell


Robert Pike

Williamsburg, VA
May 1, 2019

Broader Impacts

Arguably, the most important piece of personal protective equipment (PPE) a firefighter wears is the fire helmet. Fire helmets protect firefighters' heads from falling debris, heat, and other environmental hazards they face when they enter structure fires.

Most modern fire helmets are made from a plastic because plastic is impact resistant, durable, and affordable. However, plastic softens and deforms at temperatures between 100-200°C. While this makes plastic a less than ideal material for fire helmets, there are no other materials currently available that can rival the impact resistance and affordability that plastic provides. This is why plastic fire helmets are still being made and used today.

Unless the helmet incurs obvious damage, fire helmets can be used for up to ten years without replacement. However, this figure may not be representative of the true lifespan of the fire helmet. Surely, years of prolonged exposure to high temperatures must have an effect on the fire helmet, even if the effects occur on the molecular level.

One way to study the damage incurred by fire helmets and other materials is a technique called single-sided nuclear magnetic resonance (NMR). Single-sided NMR uses magnets and radio waves to capture information about the physical properties of materials on the molecular level. As a technique, single-sided NMR is also non-destructive, which lends itself nicely to long-term studies.

Information about plastic and how plastic changes as a result of heat exposure, even at the molecular level, will go extraordinary lengths in the fire and rescue service. This additional information may help fire helmet manufacturers engineer better products and, more importantly, influence new policies that can better protect firefighters in the line of duty.

Abstract

Many commonly used polymers are inherently flammable. Manufacturers have been able to make polymers more flame-resistant by incorporating additives in polymer matrices. Current testing methods of these materials are destructive. As a result, there is a lack of data that can characterize the long-term effects of thermal exposure on these materials. This study presents single-sided NMR as an alternative technique to characterize the physical properties of these materials before and after thermal exposure. From single-sided NMR, this study finds that it is possible to characterize the molecular behavior of flame-resistant polymers and that additives cause no significant physical change to the polymer matrix. This study also finds that single-sided NMR data can detect changes in the molecular behavior of these materials. This research emphasizes the use of single-sided NMR to study flame-resistant polymers and may prompt further study in fields such as firefighter health and safety.

Table of Contents

Acknowledgements	iv
List of Tables	vi
List of Figures	vii
1. Introduction	1
2. Polymer Chemistry	5
2.1 Fire Cycle and Suppression	
2.2 Flame-resistant Additives	
2.3 Acrylonitrile Butadiene Styrene (ABS)	
2.4 Magnesium Hydroxide	
3. NMR Theory	9
3.1 Quantum Mechanics	
3.2 Single-sided NMR Theory	
3.3 T_2 Relaxation	
4. Methodology	13
4.1 Instrumentation	
4.2 Sample Preparation	
4.3 Experimentation	
4.4 Data Processing	
5. Results and Discussion	23
6. Conclusions	33
Appendices	34
Bibliography	47

Acknowledgements

First, and most of all, I would like to thank Dr. Tyler Meldrum for all of his guidance and patience, not only throughout this investigation but for the entirety of my undergraduate career. Without his tolerance and care over the years, this thesis would not have been possible.

I would like to thank my committee members Dr. Carey Bagdassarian, Dr. Nathanael Kidwell, and Dr. Robert Pike. Your close readings and criticisms of this manuscript are greatly appreciated.

I would like to thank the members of the Meldrum research group for their supporting work on this project and always brightening my day whenever I came to work.

I would like to thank the Roy R. Charles Center for Academic Excellence at The College of William & Mary for fellowship funding.

I would like to thank the members of the Ashburn Volunteer Fire & Rescue Department. You are more than friends to me, you are family. You have all pushed me to be the better, not only as a provider but as a person. For that, I am forever grateful.

Lastly, I would like to thank my parents, Shunichi and Noriko Tsutsui. Without your unwavering support and unconditional love, nothing would be possible.

List of Tables

1. Flame test data for 3D printed ABS samples	34
2. Flame test data for ABS samples cast from acetone	35
3. Flame test data for ABS samples with 3% Mg(OH) ₂	36
4. Flame test data for ABS samples with 9% Mg(OH) ₂	37
5. Flame test data for ABS samples with 15% Mg(OH) ₂	38
6. Median T_2 values of all ABS samples and the differences between median values	39

List of Figures

1. Acrylonitrile butadiene styrene (ABS) chemical structure	8
2. The CPMG pulse sequence	12
3. Photograph of PM5 and sample	15
4. ABS samples studied	16
5. Bunsen burner flame in accordance to NFPA 1971	17
6. Flame tested 3D printed ABS samples	18
7. Flame tested ABS samples cast from acetone	18
8. Flame tested ABS samples with 3% Mg(OH) ₂	19
9. Flame tested ABS samples with 9% Mg(OH) ₂	19
10. Flame tested ABS samples with 15% Mg(OH) ₂	20
11. Single-sided NMR data for unheated ABS sample cast from acetone	21
12. Single-sided NMR data for heated ABS sample cast from acetone	22
13. Signal amplitude and T_2 relaxation results for 3D printed ABS samples	24
14. Signal amplitude and T_2 relaxation results for ABS samples cast from acetone before thermal exposure	25
15. Signal amplitude and T_2 relaxation results for ABS samples with 3% Mg(OH) ₂ before thermal exposure	25
16. Signal amplitude and T_2 relaxation results for ABS samples with 9% Mg(OH) ₂ before thermal exposure	26
17. Signal amplitude and T_2 relaxation results for ABS samples with 15% Mg(OH) ₂ before thermal exposure	26

18. Signal amplitude and T_2 relaxation results for ABS samples after thermal exposure	35
19. Signal amplitude and T_2 relaxation results for ABS samples with 3% $Mg(OH)_2$ after thermal exposure	36
20. Signal amplitude and T_2 relaxation results for ABS samples with 9% $Mg(OH)_2$ after thermal exposure	37
21. Signal amplitude and T_2 relaxation results for ABS samples with 15% $Mg(OH)_2$ after thermal exposure	38

1. Introduction

Firefighter personal protective equipment (PPE) refers to the clothing and equipment that firefighters wear to protect themselves from hazards they face in the line of duty. [1] Most modern fire helmets are made of thermoplastic or fiberglass. Thermoplastic fire helmets are typically made of polycarbonate. Other thermoplastics may also be used, but manufacturer guidelines do not outline which ones are used in place of polycarbonate. Polycarbonate fire helmets are popular due to their high impact resistance. However, polycarbonate and other thermoplastics are weak against thermal and chemical exposure. Polycarbonate, for instance, softens at 150°C and deforms at 200°C. The thermal capacity of fire helmets is increased by increasing the thermoplastic shell thickness. [2, 3] The thicker the plastic shell, the heavier the helmet becomes. The heaviness of the helmet has caused firefighters to complain of neck pain after prolonged wear. [4]

The National Fire Protection Association (NFPA) develops and maintains codes and standards for usage and adoption by federal, state, county, and municipal governments in the United States. NFPA 1851 is the current standard that is used to outline the selection, care, and maintenance of firefighter PPE. According to the most recent edition of NFPA 1851, all PPE—turnout coats, turnout pants, protective hoods, gloves, fire boots, and helmets—must be retired ten years after manufacture. [5] The service life timeline of firefighter PPE is dictated by the weathering of the textile products, with almost no consideration for the life span other materials. [6] While all PPE is tested for heat resistance and degradation, all testing is only done at high temperatures, where obvious deformity can be seen. There is no data that describes the properties of these materials after exposures at intermediate temperatures or when other invisible damage is incurred. [1] All current testing methods are also destructive and are not conducive for long-term

studies. [6, 7] Heat resistance and degradation of PPE materials are also only rigorously tested during the initial testing phase that determines if the PPE meets the NFPA guidelines. PPE is not closely regulated or monitored after initial testing. [8]

Due to a lack of current data on polymers used for fire helmets and a maintenance standard that does not account for the material life spans of these polymers, PPE replacements are seen as arbitrary and unnecessarily pushed by manufacturers, even though the true performance capabilities of the PPE are still unknown. [1]

In addition to protecting the health and safety of firefighters, it is important to understand not only the material life spans of polymers, but the physical properties of these materials due to their prevalence in modern life. Polymers are used in a variety of industries for a number of applications and as a result are constantly being improved through research and development activities.

One popular area of research in polymer science is flame-resistance. Most commonly-used polymers are inherently combustible due to their chemical composition. Since the nineteenth century, reducing material flammability has been an area of interest with the discoveries and uses of nitrocellulose and celluloid in photography. However, it has only been in recent decades that flame-resistant polymers have been formulated to not only reduce flammability but to also reduce the risks of producing smoke and toxic fumes. While intrinsically flame-resistant polymers can be synthesized, flame-resistant polymers are more commonly made flame-resistant by mixing in flame-resistant additives with a base polymer during manufacturing. These additives are engineered to reduce polymer flammability by interfering with the chemical and physical mechanisms aspects of material combustion. [9]

Across all industries, current methods to test the efficacy of flame-resistant polymers require flame tests. [9] From flame tests, characteristics such as ignition resistance, flame spread, duration of afterflame and afterglow, burn patterns, and smoke and toxic gas output can be determined. These results determine whether or not the polymer is safe for manufacture and mass consumption. [7, 10] Quantitative and qualitative studies of these polymers tend to also employ thermo-analytical methods such as thermogravimetric analysis (TGA) and temperature program pyrolysis (TPPy) paired with detection methods such as gas chromatography and mass spectrometry, which are all destructive analytical techniques. [11] While the data collected using these methods are valuable, these testing methods are not compatible with for use with long-term studies, as reflected by the limited data on the effects of thermal exposure on these polymers over time.

Nuclear magnetic resonance spectroscopy (NMR) is an analytical technique that has the capability to identify and characterize molecules by measuring the energy difference between nuclear spin states. In contrast to other analytical techniques, NMR is non-destructive, making the technique suitable for long-term studies. However, the types of samples that can be studied using NMR are drastically limited and sample preparation for NMR studies can also be invasive and destructive to source material. [12]

Single-sided NMR is an alternative method that can overcome some of the drawbacks of traditional NMR. By using permanent magnets instead of superconducting magnets, single-sided NMR has an open geometry that allows the study of large and irregularly shaped samples. [12] Like traditional NMR, single-sided NMR is also a non-destructive technique, making single-sided NMR conducive to long-term studies. Though the ability to collect detailed information such as chemical shift data is lost due to the inhomogeneous magnetic field that results from the

use of a permanent magnet, other information such as transverse relaxation (T_2 relaxation) can still be measured with single-sided NMR by using the Carr-Purcell-Meiboom-Gill (CPMG) pulse sequence. T_2 relaxation times can characterize the physical properties of materials such as cross-linking and rigidity. [13]

In this study, single-sided NMR is used to characterize the physical properties of flame-resistant polymers before and after thermal exposure. This will help supplement existing data on flame-resistant materials. In addition, this study will demonstrate how single-sided NMR is a good candidate for analyzing not only flame-resistant polymers, but other flame-resistant materials, especially for analyzing these materials over time.

2. Polymer Chemistry

2.1 Fire Cycle and Suppression

The fire cycle begins when a material is ignited. Ignition can occur either in the presence of an external heat source or automatically if the material has reached a sufficient temperature to overcome the activation energy of the combustion reaction. Once ignited, the material will decompose into flammable products—flammable gases and liquids and tar—and non-flammable products—non-flammable gases, smoke, and solids. As the flammable products are produced, they interact with atmospheric oxygen, setting off a chain of reactions allow the flame to become self-sustaining. [9]

As the flame burns, it releases heat and causes the temperature of the material and surroundings to climb. If the flame is left to grow for long enough, the surroundings are liable to flashover or spontaneously ignite. At the peak temperature and heat release rate, a fire is considered fully developed. Eventually, the fire will start to decay once all combustible materials have been consumed. Consequently, the temperature and heat release rate of the fire will fall, leaving the non-flammable products to smolder and the fire to eventually self-extinguish. [9]

The fire cycle can be disrupted by the following mechanisms: directly inhibiting the chemical reactions occurring in the flame, cooling the material, and preventing material decomposition. Flame-resistant additives are designed to employ one or more of these mechanisms. This results in three different types of commercially available flame-resistant additives: radical, char-forming, and endothermic. [9]

2.2 Flame-resistant Additives

Radical additives are typically halogenated compounds that release halogen free radical scavengers when heated. These free radical scavengers are meant to target the free radicals that are produced by flames, such as hydrogen and hydroxyl radicals. When the scavengers bind with their targets they form non-flammable compounds, ultimately inhibiting material combustion. For decades, radical additives like tetrabromobisphenol-A (TBBPA) were the most commonly used in flame-resistant polymer formulations because they were affordable, easy to produce, and versatile. However, due to their persistence in the environment due to bioaccumulation and their known contributions to adverse health effects, radical additive production and use in polymer formulations have become regulated and have fallen out of favor with the general public. [9, 14]

Char-forming additives are typically nanocomposites or phosphorus-containing compounds like ammonium polyphosphate (APP). Upon heating, char-forming additives will promote the material to char. When a material chars, a thick and glossy carbon layer is formed on a material surface. The layer of carbon insulates the material and provides protection between the flame and the material. This prevents further thermal degradation of the material. [9]

Endothermic additives are typically metal hydroxides, nitrogen-containing compounds, or carbonates. These additives have become increasingly popular in flame-resistant polymer formulations because they are non-toxic, non-corrosive, and affordable. Upon heating, endothermic additives will generate gases like water vapor, nitrogen, and carbon dioxide. Unlike many other gases, the gases that are generated by these additives have high heat capacities. With the release of these gases, heat that is being generated during combustion will be absorbed, lowering the temperature of the material and the surroundings. Also, due to their non-flammable nature, these gases will not undergo combustion reactions. Material combustion, as a result, is

slowed as the activation energy barrier for combustion reactions becomes harder for the system to overcome. Flames will then burn at a slower rate and eventually, flames will be able to self-extinguish. In addition to absorbing heat, the release of these gases prevents combustion reactions from occurring by diluting the flammable gases being produced by the flame and decreasing the likelihood of these flammable gases from reacting with atmospheric oxygen. [9]

2.3 Acrylonitrile Butadiene Styrene (ABS)

Acrylonitrile butadiene styrene (ABS) is another widely used thermoplastic due to its strength against chemicals and good impact resistance. The chemical structure of ABS is provided in Figure 1.

ABS, however, is also inherently flammable. [15] Traditionally, ABS was made more flame-resistant by incorporating halogenated additives in its formulations. More recent flame-resistant formulations of ABS employ phosphate-containing additives like triphenyl phosphate (TPhP). TPhP and its analogues, however, are not ideal alternatives to use in large-scale manufacturing because they are liquids and evaporate and decompose at too low of a temperature to be incorporated in ABS resins. Researchers are still developing novel additives that not only increase the flame-resistance of ABS but are also compatible for use in large-scale manufacturing. [16]

ABS was used as the base polymer in this study as a more affordable alternative to polycarbonate. ABS was also chosen over other high impact resistant thermoplastics due to its ease in casting.

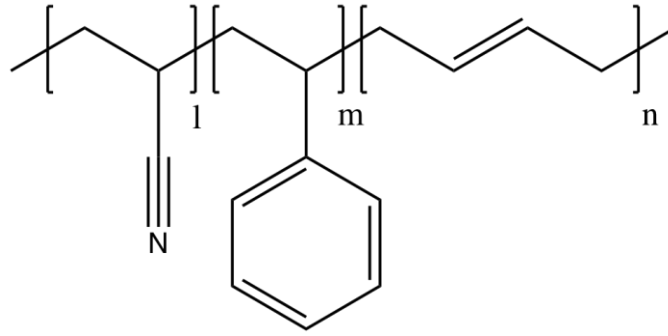


Figure 1: Chemical structure of acrylonitrile butadiene styrene (ABS). l , m , and n refer to the variable lengths of the monomer units that make up the ABS polymer strand.

2.4 Magnesium Hydroxide

Magnesium hydroxide, also known as magnesium dihydroxide (MDH), has become increasingly popular in flame-resistant polymer formulations because it is non-toxic, non-corrosive, and affordable. Magnesium hydroxide is an endothermic additive, as it produces water vapor and magnesium oxide when it thermally decomposes, as shown below:



In addition to its ability to absorb heat, water vapor also acts as a smoke suppressant. While the mechanism is still not known, water vapor has also been shown to reduce the amount of carbon monoxide produced from polymer combustion. [9]

Magnesium hydroxide was used as the flame-resistant additive in this study due to its potential as a flame-resistant additive and smoke suppressant for large-scale manufacturing and its affordability.

3. NMR Theory

3.1 Quantum Mechanics

NMR observes resonance, a physical phenomenon that characterizes the behavior of atomic nuclei when they are placed in an applied magnetic field and perturbed with electromagnetic radiation, typically at radio frequency. All nuclei have an intrinsic nuclear spin. However, only nuclei with a non-zero spin quantum number can be probed with NMR, as only nuclei with non-zero spin quantum numbers will have a net nuclear spin angular momentum and magnetic moment when placed in an applied magnetic field, which is referred to as precession. The nuclei precess at the Larmor or resonance frequency, which is proportional to the applied magnetic field as shown in the Larmor frequency equation below:

$$\omega = \gamma B_0$$

where ω is the Larmor frequency in radians, γ is the gyromagnetic ratio of the nucleus of interest, and B_0 is the magnitude of the applied magnetic field. The most common nuclei that are probed using NMR are ^1H and ^{13}C , which both have a spin quantum number of $\pm 1/2$. [17]

When nuclei are placed in an applied magnetic field, the spins will also align either parallel or antiparallel to the magnetic field. The rearrangement of spins into parallel and antiparallel populations creates an energy gap. This is in accordance to the Boltzmann distribution, given below:

$$\frac{p_{\text{antiparallel to } B_0}}{p_{\text{parallel to } B_0}} = e^{-\Delta E/kT}$$

where k is the Boltzmann constant, T is the temperature in Kelvin, and ΔE is the energy gap.

While the population difference between the nuclei is small, there are still more nuclei that are parallel to the applied magnetic field than antiparallel, as it is slightly more energetically favorable for spins to be in line with the magnetic field. This results in a bulk magnetization

vector that is parallel to the applied magnetic field. The bulk magnetization vector is designated along the z-axis. The differences in energy between the two populations is what gives rise to NMR signal. The stronger the applied magnetic field is, the greater the difference is between the parallel and antiparallel population, resulting in stronger and more intense NMR signal. [17]

Traditional NMR experiments are conducted using superconducting electromagnets, which create a strong, homogenous applied magnetic field. This allows for the collection of detailed structural information such as chemical shift data, which can later aid in tasks like structure elucidation. While valuable, traditional NMR instruments are expensive and high-maintenance, requiring the use of liquid nitrogen and helium in order to keep the superconducting electromagnets functional. This results in a bulky, stationary instrument. The size and shape of the sample holder for these magnets restrict the types of samples that can be measured with traditional NMR. The placement of the sample holder in the bore of the magnet also makes the sample inaccessible during measurements. [12]

3.2 Single-sided NMR Theory

Single-sided NMR was developed as an alternative that overcomes some of the drawbacks posed by traditional NMR instrumentation. In place of superconducting electromagnets configured in a cylindrical shape, single-sided NMR instruments uses permanent magnets that are kept planar. The open geometry that single-sided NMR offers makes it an ideal candidate to measure large and irregularly shaped samples. The open geometry also eliminates the need for potentially invasive and damaging sample preparation methods. Also, because it is a non-destructive analytical technique, single-sided NMR has successfully been used to analyze cultural heritage objects, buildings, and food. [12]

Simplifying the instrumentation, however, comes with a cost. The use of permanent magnets results in a weaker, inhomogeneous magnetic field. The inhomogeneities in the field eliminates the ability to gather detailed structural information. [12] However, parameters that can be obtained using traditional NMR can still be obtained using single-sided NMR, for example transverse relaxation.

3.3 T_2 Relaxation

Transverse relaxation (T_2 relaxation) is a parameter that describes the amount of time it takes for nuclear spins in the transverse plane (x, y-plane) to dephase. [17] On single-sided NMR instruments, T_2 relaxation is measured using the Carr-Purcell-Meiboom-Gill (CPMG) pulse sequence. [13]

When measuring T_2 relaxation times using the CPMG pulse sequence, the nuclei that are parallel to the magnetic field, along the z-axis, are knocked into the x, y-plane with a $\pi/2$ pulse. Once in the x, y-plane, the nuclei will induce a current, known as the free induction decay (FID). This current can then be detected by a detector coil in a spectrometer. The nuclei in the x, y-plane will then be struck by iterative refocusing π pulses. The iterative refocusing pulses will create a series of echoes that will appear spaced out at regular time intervals. Over time, the echoes will decrease in signal amplitude due to spin decoherence. Measuring the signal decay of the echo train will then be used to determine the T_2 relaxation. [12]

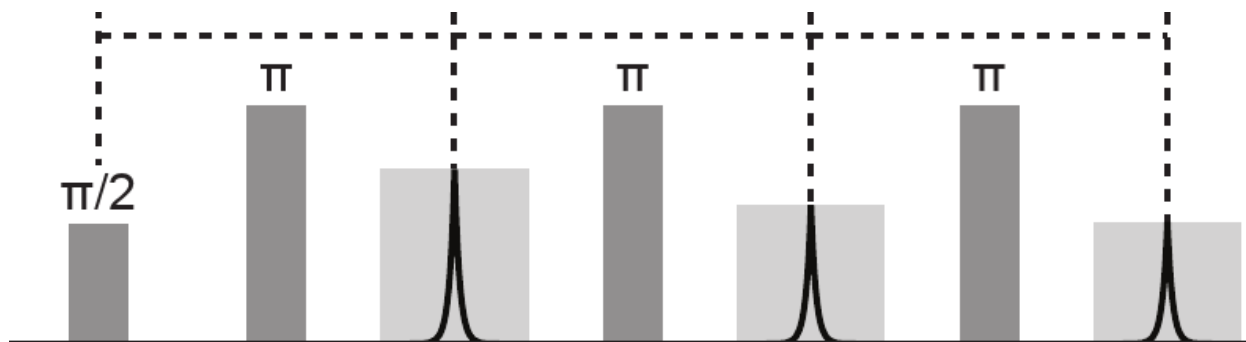


Figure 2: Schematic of the CPMG pulse sequence. The $\pi/2$ pulse places all of the nuclei that were along the z-axis into the x, y-plane. The iterative π refocusing pulses generate detectable echoes. The echoes over time decay. The echo decay train is then used to determine the T_2 relaxation.

The smaller the T_2 relaxation time, the less molecular motion is present in the sample.

[13] In the context of polymers, a smaller T_2 relaxation time for a polymer sample corresponds to a sample that has less molecular motion. The more that spins interact with each other, the faster spin decoherence occurs. Physically, this translates into a more rigid polymer and shows evidence of greater crosslinking and residual dipolar coupling present in the sample. As the polymer network becomes more disrupted, there should be evidence of greater molecular motion and, therefore, larger corresponding T_2 relaxation times.

4. Methodology

4.1 Instrumentation

All NMR measurements were done on the PM5, a single-sided NMR magnet with a field strength of about 0.4 T and a field gradient of 23.5 T/m, connected to a Kea2 spectrometer. Both the PM5 and the Kea2 spectrometer are produced by Magritek.

The sensitive region of the magnet, which is directly above the radio frequency coil, can measure sample areas up to 25 mm by 25 mm. The maximum depth within a sample that the sensitive region can probe is 5 mm. The maximum depth can be altered with the insertion of up to two, 2 mm spacers in the magnet. While adding spacers decreases the maximum depth, the amount of signal that can be detected by the magnet increases. Adding in the spacers also shortens the pulse length and minimum echo times that can be used during CPMG experiments.

The magnet is also attached to a mechanised lift that can move the magnet up or down by 10 or 50 μm increments. The lift allows for the user to optimize the magnet's position to ensure that the region of the sample with the greatest signal density is being probed.

The magnet, spectrometer, and lift are all connected to a laptop that runs software called Prospa, which is also produced by Magritek. In Prospa, the signal output generated by experiments is recorded.



Figure 3: The PM5 in the mechanical lift and the Kea2 spectrometer with an ABS sample atop the sensitive region on the magnet. For deformed samples, glass slides were used to stabilize the sample, keeping the sample flush with the sensitive region for the duration of the T_2 experiment.

4.2 Sample Preparation

Four types of samples were studied: 3D printed ABS filament, ABS cast from acetone, ABS with 3% magnesium hydroxide by weight, ABS with 9% magnesium hydroxide by weight, and ABS with 15% magnesium hydroxide by weight.

The 3D printed ABS samples were printed from a nozzle temperature of 235°C at 100% fill. The samples were printed at 0.3 mm thickness with an area of 25 mm by 25 mm.

ABS samples cast from acetone were prepared first by mixing ABS and acetone in a 10 to 1 ratio of acetone to ABS by weight in an Erlenmeyer flask. The resultant slurry was then heated at 35°C on a hot plate with the mouth of the Erlenmeyer flask topped with a watch glass. As it was heating, the slurry was stirred constantly using a magnetic stir bar. The slurry was

heated and stirred until all of the ABS dissolved in the acetone. The ABS slurry was cast out into preweighed aluminum weigh boats. The samples were then left to dry at ambient temperature and pressure until the masses of the samples stabilized, indicating that the maximum amount of acetone had evaporated from the samples.

ABS with magnesium hydroxide samples were prepared by mixing ABS, magnesium hydroxide of weight equal to 3, 9, or 15% of ABS, and acetone in a 10 to 1 ratio of acetone to the total weight of ABS and magnesium hydroxide in an Erlenmeyer flask. Sulfuric acid was then added dropwise to the slurry using a Pasteur pipette (less than 1% of the total volume of acetone used) to homogenize the ABS slurry and the magnesium hydroxide. The resultant slurry was then heated at 35°C on a hot plate with the mouth of the Erlenmeyer flask topped with a watch glass. As it was heating, the slurry was stirred constantly using a magnetic stir bar. The slurry was heated and stirred until all of the ABS dissolved in the acetone and all of the magnesium hydroxide remained suspended in the slurry once the stir bar was turned off. The ABS slurry was cast out into preweighed aluminum weigh boats. The samples were then left to dry at ambient temperature and pressure until the masses of the samples stabilized, indicating that the maximum amount of acetone had evaporated from the samples.



Figure 4: ABS samples studied. From left to right: 3D printed ABS filament, ABS cast from acetone, ABS with 3% $\text{Mg}(\text{OH})_2$ by weight, ABS with 9% $\text{Mg}(\text{OH})_2$ by weight, ABS with 15% $\text{Mg}(\text{OH})_2$ by weight.

4.3 Experimentation

All T_2 measurements were determined by CPMG experiments that were performed on the PM5. All CPMG experiments were measured with a pulse length of $2.75 \mu\text{s}$ for the 90° and 180° pulses, pulse amplitudes of -4 for the 180° pulse and -10 for the 90° pulse, and an echo time of $40 \mu\text{s}$. During the $40 \mu\text{s}$ echo time, 512 echoes were collected. A total of 512 acquisition scans were used, yielding a total T_2 measurement time of 8 minutes and 30 seconds. All of the experimental parameters for the CPMG sequence are outlined in Appendix B.

Each sample was measured by a set of three CPMG experiments. The set of CPMG experiments were measured using a script that was developed in-house to run experiments in succession. The experimental parameters were preloaded and saved in the script before it was run through the debugger in Prospa. The debugger script is provided in Appendix B.

All flame tests were performed with a Bunsen burner. The burner flame was adjusted to match the flame specifications outlined in the test methods section of NFPA 1971. The resultant flame was approximately 1200°C . The ABS samples were placed against the inner cone of the

flame for 1, 3, or 5 seconds before being removed from the flame. If the sample caught fire, the sample was left to burn until the flame self-extinguished. The time until the the flame self-extinguished was also recorded.

Flame test data for all samples can be found in Tables 1-5 in Appendix A.



Figure 5: Bunsen burner flame set up as outlined in the test methods section of NFPA 1971.¹ The inner cone is about 25 mm in height and the outer cone is approximately 50 mm in height. The resultant flame is approximately 1200°C.

¹ NFPA 1971 (2018) states the following in Chapter 8 (Test Methods) on pp 51: “The flame of the Bunsen burner shall be adjusted to produce a 50 mm ± 1.5 mm (2 in. ± 1/16 in.) blue flame with an inner cone of 25 mm ± 1.5 mm (1 in. ± 1/16 in.)”

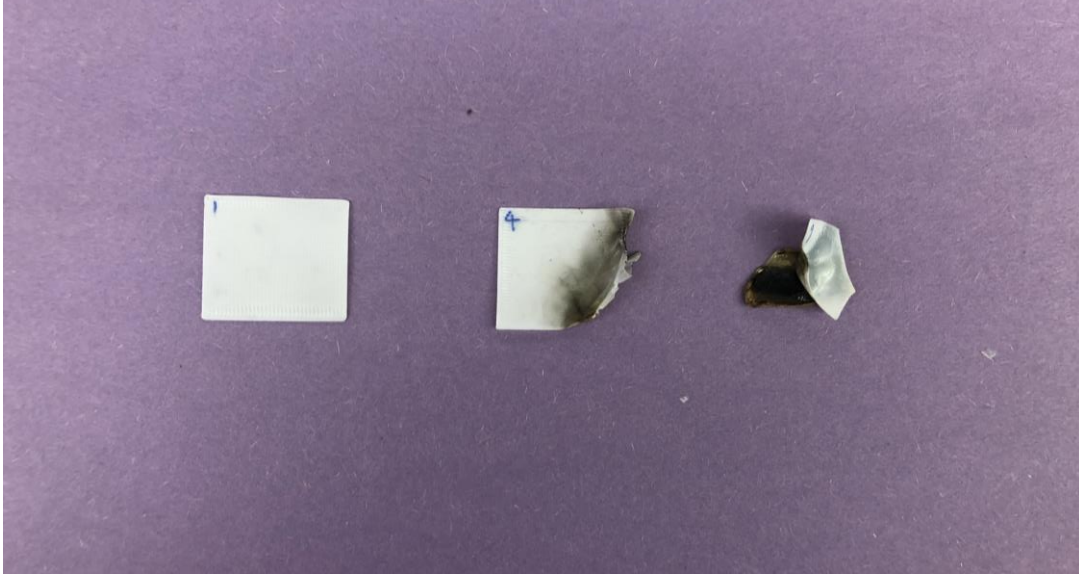


Figure 6: Flame tested 3D printed ABS filament samples. From left to right: 1 second of thermal exposure, 3 seconds of thermal exposure, and 5 seconds of thermal exposure.



Figure 7: Flame tested ABS samples cast from acetone. From left to right: 1 second of thermal exposure, 3 seconds of thermal exposure, and 5 seconds of thermal exposure.



Figure 8: Flame tested ABS samples with 3% Mg(OH)₂ by weight. From left to right: 1 second of thermal exposure, 3 seconds of thermal exposure, and 5 seconds of thermal exposure.



Figure 9: Flame tested ABS samples with 9% Mg(OH)₂ by weight. From left to right: 1 second of thermal exposure, 3 seconds of thermal exposure, and 5 seconds of thermal exposure.



Figure 10: Flame tested ABS samples with 15% Mg(OH)₂ by weight. From left to right: 1 second of thermal exposure, 3 seconds of thermal exposure, and 5 seconds of thermal exposure.

4.4 Data Processing

All single-sided NMR data was processed in MATLAB using a script that was developed in-house.

The processing script integrates the area under each echo in the full echo train, calculating the sum of the signal intensity for each echo. The resultant signal intensities for each echo are then plotted and fitted to a monoexponential, biexponential, and triexponential decay curves of the form:

$$S(t) = Ae^{-t/T_2}$$

$$S(t) = Ae^{-t/T_{21}} + (1 - A)e^{-t/T_{22}}$$

$$S(t) = A_1e^{-t/T_{21}} + A_2e^{-t/T_{22}} + (1 - A_1 - A_2)e^{-t/T_{23}}$$

where S is the signal intensity and t is the time in seconds. $T_2(1)$, $T_2(2)$, and $T_2(3)$ are the unique T_2 values observed. In the monoexponential decay curve, A is the signal intensity attributed to T_2 . In the biexponential decay curve, A is the signal intensity attributed to $T_2(1)$ and (1-A) is the signal intensity corresponding to $T_2(2)$. In the triexponential decay curve, A_1 is the signal

intensity attributed to $T_2(1)$, A_2 is the signal intensity attributed to $T_2(2)$, and $(1-A_1-A_2)$ is the signal intensity attributed to $T_2(3)$.

Fit residuals for each exponential decay curve were also plotted against time in seconds. The decay curve with the fit residuals most random about zero was determined to be the best fit for the data set.

The processing script is provided in Appendix C.

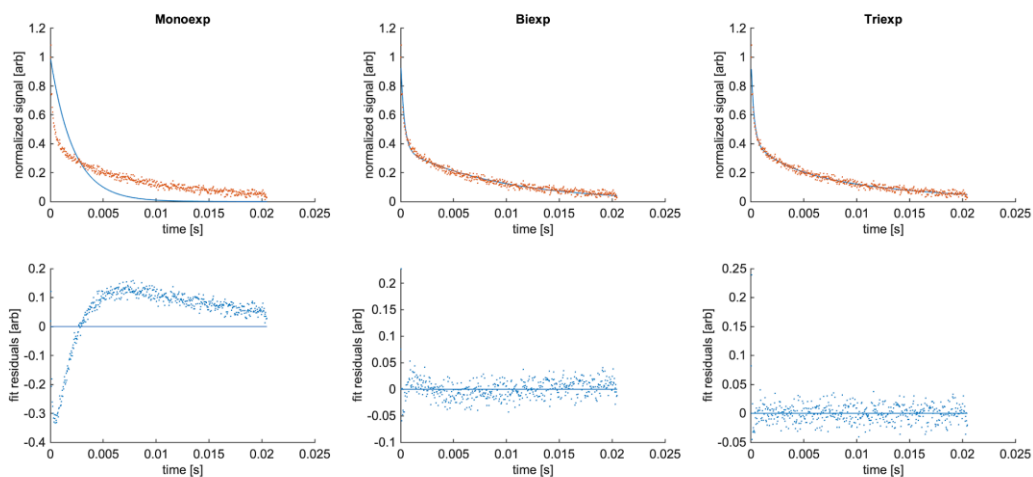


Figure 11: Single-sided NMR data of an ABS sample cast from acetone before thermal exposure. The data were fit to a monoexponential, biexponential, and triexponential decay curves with fit residual plots for each curve. The fit residuals are most random about zero when the data are fit to the triexponential curve. This indicates that the triexponential decay curve is the best fit for the data set. This also indicates that there are three T_2 relaxation times that characterize the molecular motion of the material.

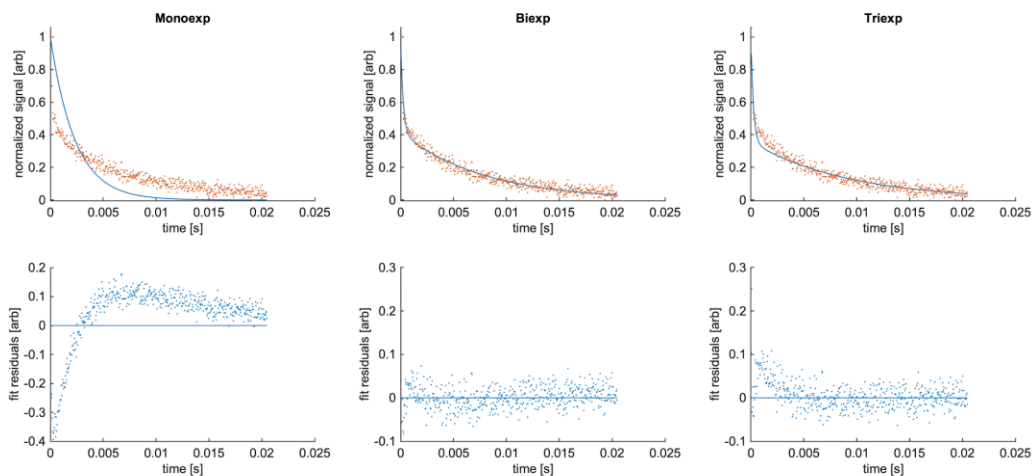


Figure 12: Single-sided NMR data of an ABS sample cast from acetone after thermal exposure. The data were fit to a monoexponential, biexponential, and triexponential decay curves with fit residual plots for each curve. The fit residuals are most random about zero when the data are fit to the biexponential curve. This indicates that the biexponential decay curve is the best fit for the data set. This also indicates that there are two T_2 relaxation times that characterize the molecular motion of the material.

5. Results and Discussion

All single-sided NMR data for the 3D printed ABS tiles were biexponential in nature, meaning two unique T_2 relaxation times were detected. Figure 13 shows the boxplots of the normalized signal amplitudes and T_2 relaxation values for the 3D printed ABS samples. The median values for both of the large and small T_2 relaxation times remained consistent, both before and after thermal exposure, though the range of T_2 values does broaden after flame testing. This indicates that while visually, the samples appear to have changed, there is no evidence that the ABS sample has changed at the molecular level. While it is unknown why this trend occurred, most likely it is due to the fact that these samples were extruded rather than cast from solvent. The 3D printed ABS strands probably annealed and differently than the ABS strands that were cast from acetone.

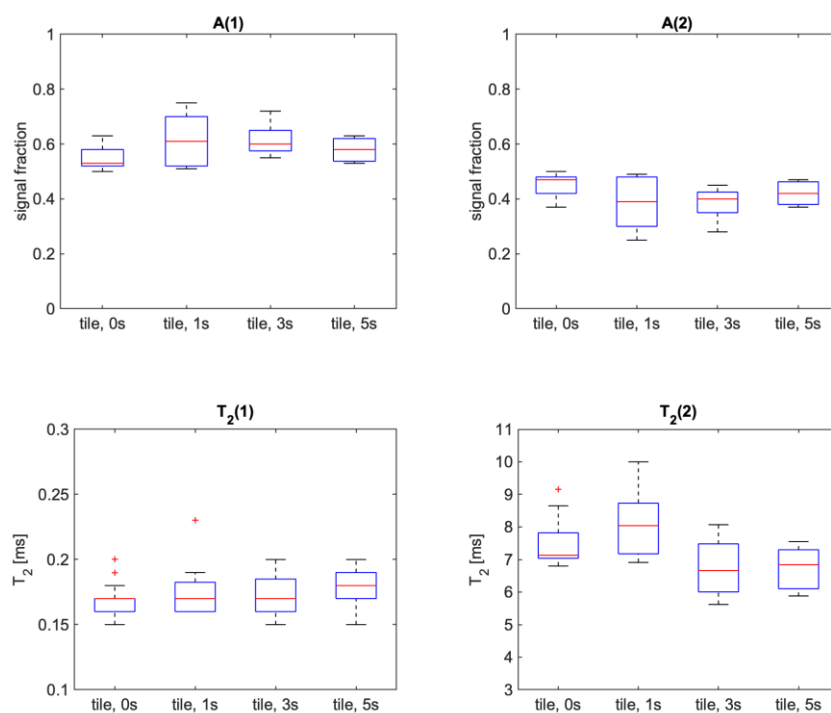


Figure 13: Normalized signal amplitudes (arbitrary units) and T_2 relaxation times (ms) for 3D printed ABS filament samples before and after thermal exposure. 19 samples total (10 samples flame tested, 9 samples untested).

All single-sided NMR data for the ABS samples originally cast from acetone—regardless of the amount of $\text{Mg}(\text{OH})_2$ present—were triexponential in nature before thermal exposure, meaning three unique T_2 relaxation times were detected. Most likely, the appearance of the third T_2 component and its corresponding signal amplitude in these samples is due to residual acetone trapped in the ABS polymer network. The residual acetone solvates the subunits along the ABS polymer strands and promotes additional rotational motion about the strands and translational motion between the strands, which then appear in the single-sided NMR data. Figures 14-17 show the boxplots of the normalized signal amplitudes and T_2 relaxation values for these samples before thermal exposure.

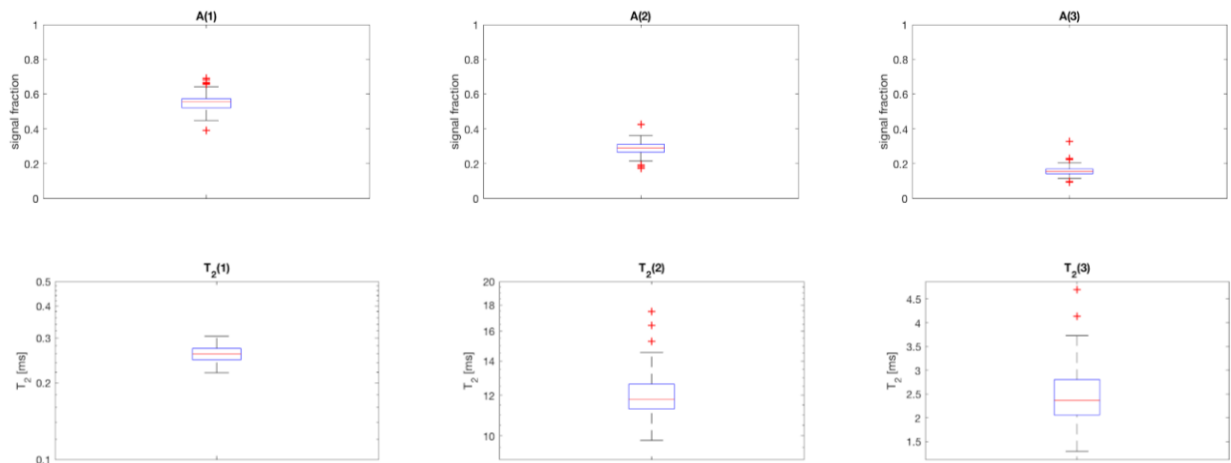


Figure 14: Normalized signal amplitudes (arbitrary units) and T_2 relaxation times (ms) for ABS samples cast from acetone with no $Mg(OH)_2$ before thermal exposure. 20 samples total.

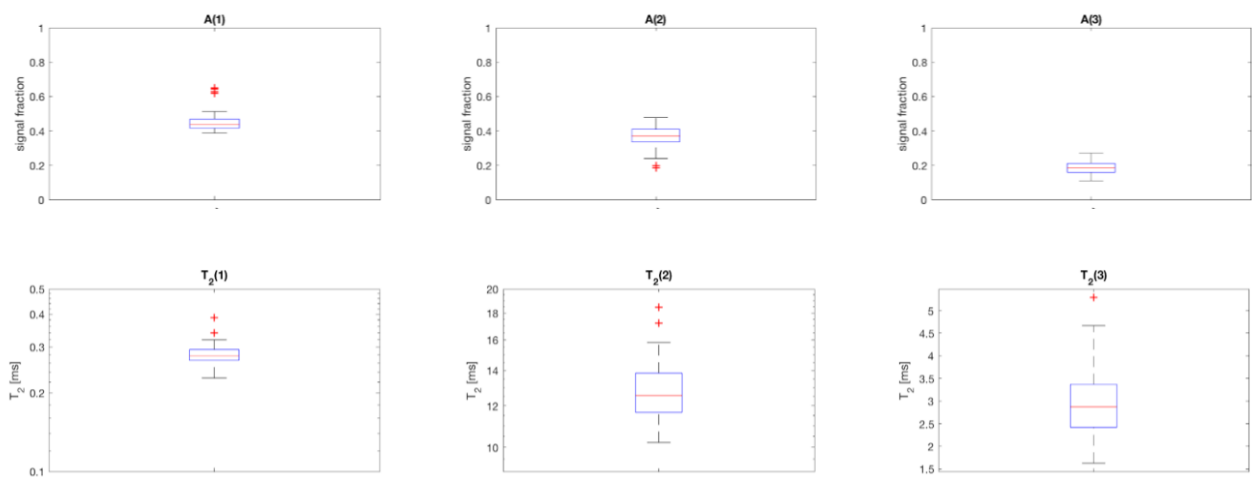


Figure 15: Normalized signal amplitudes (arbitrary units) and T_2 relaxation times (ms) for ABS samples with 3% $Mg(OH)_2$ by weight before thermal exposure. 16 samples total.

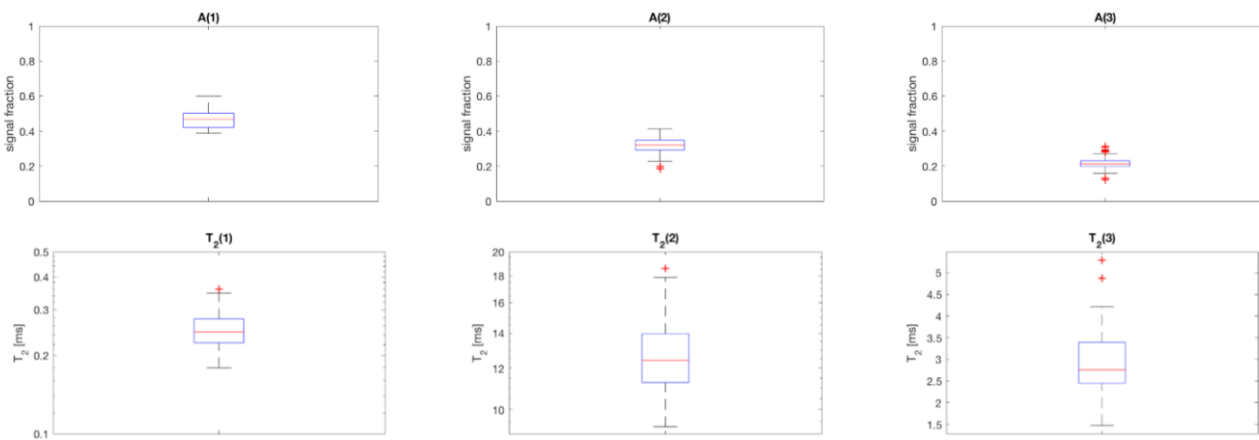


Figure 16: Normalized signal amplitudes (arbitrary units) and T_2 relaxation times (ms) for ABS samples with 9% $\text{Mg}(\text{OH})_2$ by weight before thermal exposure. 19 samples total.

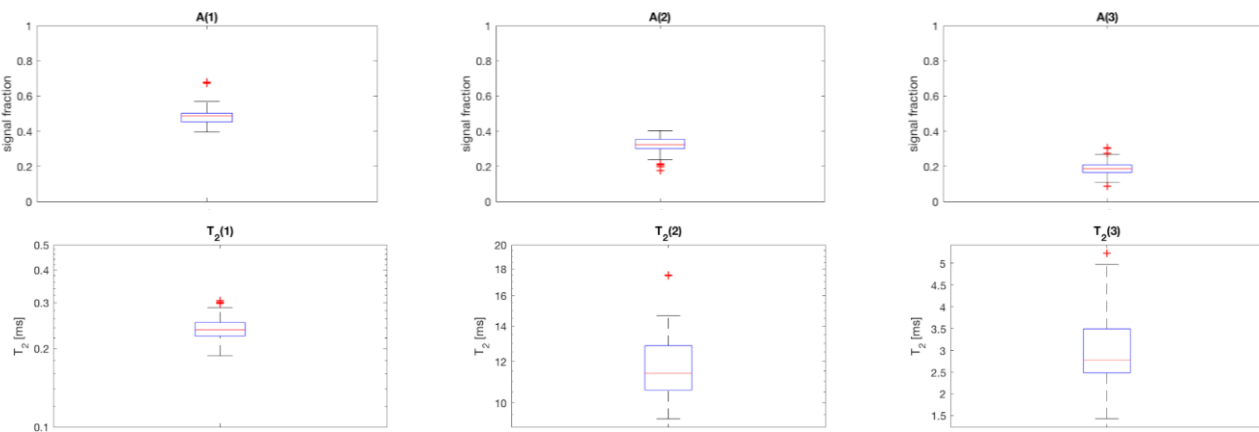


Figure 17: Normalized signal amplitudes (arbitrary units) and T_2 relaxation times (ms) for ABS samples with 15% $\text{Mg}(\text{OH})_2$ by weight before thermal exposure. 20 samples total.

All single-sided NMR data for the ABS samples originally cast from acetone, regardless of the amount of $\text{Mg}(\text{OH})_2$ present, were biexponential in nature after thermal exposure. Most likely, the disappearance of the third T_2 component and its corresponding signal amplitude is due to the residual acetone burning off during the flame tests. The solvent effects of the acetone in the ABS polymer network are lost, and therefore, the additional types of motion that were once present in these samples no longer appear in the single-sided NMR data. Figures 18-21 show the boxplots of the normalized signal amplitudes and T_2 relaxation values for these samples after

thermal exposure. Based off of the median T_2 relaxation times for these samples before thermal exposure, there is no evidence to suggest that the presence of $\text{Mg}(\text{OH})_2$ disrupts the overall ABS polymer network. The median T_2 relaxation times for these samples can be found in Table 6 in Appendix A.

Figure 18 shows the boxplots of the normalized signal amplitudes and T_2 relaxation values for the ABS samples that were cast from acetone with no $\text{Mg}(\text{OH})_2$ present. The median values for the small T_2 relaxation times decreased after 1 second of thermal exposure and decreased further after 3 seconds of thermal exposure. The median value for the small T_2 relaxation time after 5 seconds of thermal exposure is consistent with the median value for the short T_2 relaxation time observed after 3 seconds of thermal exposure. The decrease in T_2 relaxation values is indicative of more brittleness and rigidity in the ABS polymer network at the molecular level. However, the consistency between the median T_2 relaxation values after 3 seconds of thermal exposure and 5 seconds of thermal exposure suggests that after a certain point of thermal exposure, the ABS polymer has been chemically altered to the point where increased thermal exposure will not have further effects on the polymer network. The median values for the large T_2 relaxation times, remain consistent before and after thermal exposure. The differences in the median T_2 values before and after thermal exposure for these samples can be found in Table 6 in Appendix A.

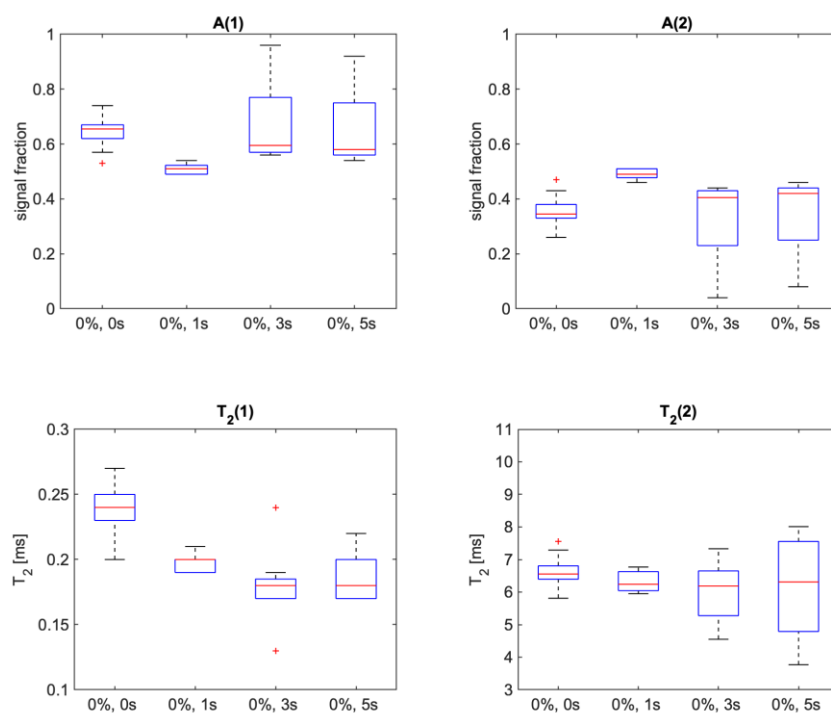


Figure 18: Normalized signal amplitudes (arbitrary units) and T_2 relaxation times (ms) for ABS samples cast from acetone with no $\text{Mg}(\text{OH})_2$ after thermal exposure. 20 samples total (10 flame tested, 10 untested).

Figure 19 shows the boxplots of the normalized signal amplitudes and T_2 relaxation values for the ABS samples with 3% $\text{Mg}(\text{OH})_2$ by weight. The median values for the small T_2 relaxation times decrease after thermal exposure, which again indicates an increase in brittleness and rigidity in the ABS polymer network. However, the amount of thermal exposure appears to be independent of the changes observed in the small T_2 relaxation times before and after thermal exposure. This suggests that the presence of $\text{Mg}(\text{OH})_2$ in the polymer network helps shield the ABS polymer network from thermal decomposition. The median values for the large T_2 relaxation times remained consistent before and after thermal exposure. The differences in the median T_2 values before and after thermal exposure for these samples can be found in Table 6 in Appendix A.

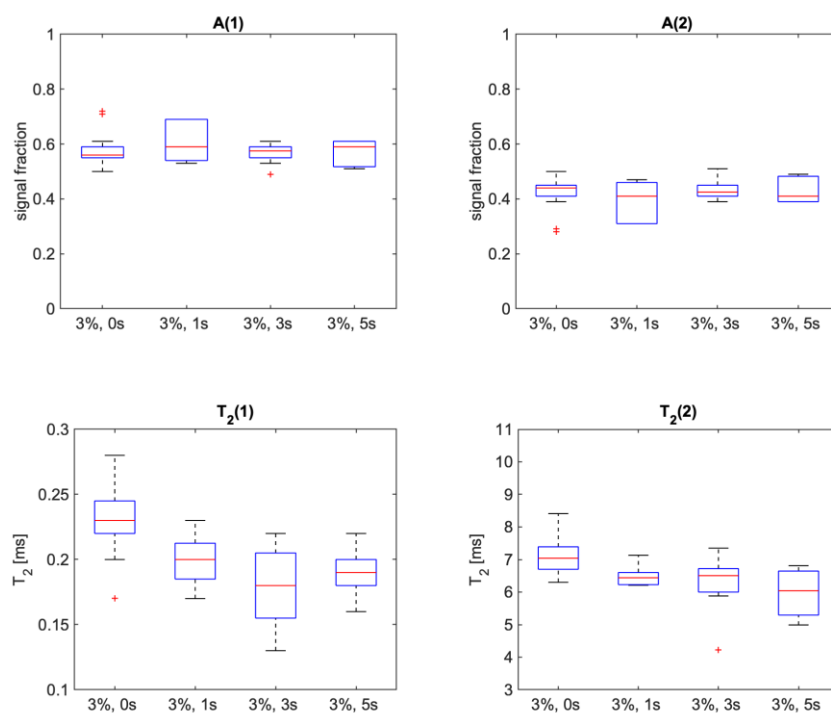


Figure 19: Normalized signal amplitudes (arbitrary units) and T_2 relaxation times (ms) for ABS samples with 3% $\text{Mg}(\text{OH})_2$ by weight after thermal exposure. 16 samples total (10 samples flame tested, 6 untested)

Figures 20 and 21 show the boxplots of the normalized signal amplitudes and T_2 relaxation values for the ABS samples with 9% $\text{Mg}(\text{OH})_2$ by weight and ABS samples with 15% $\text{Mg}(\text{OH})_2$, respectively. The median values of both the large and small T_2 relaxation times remain consistent before and after thermal exposure, further suggesting that the presence of $\text{Mg}(\text{OH})_2$ in the polymer network helps shield the ABS polymer network from thermal degradation. The differences in the median T_2 values before and after thermal exposure for these samples can be found in Table 6 in Appendix A.

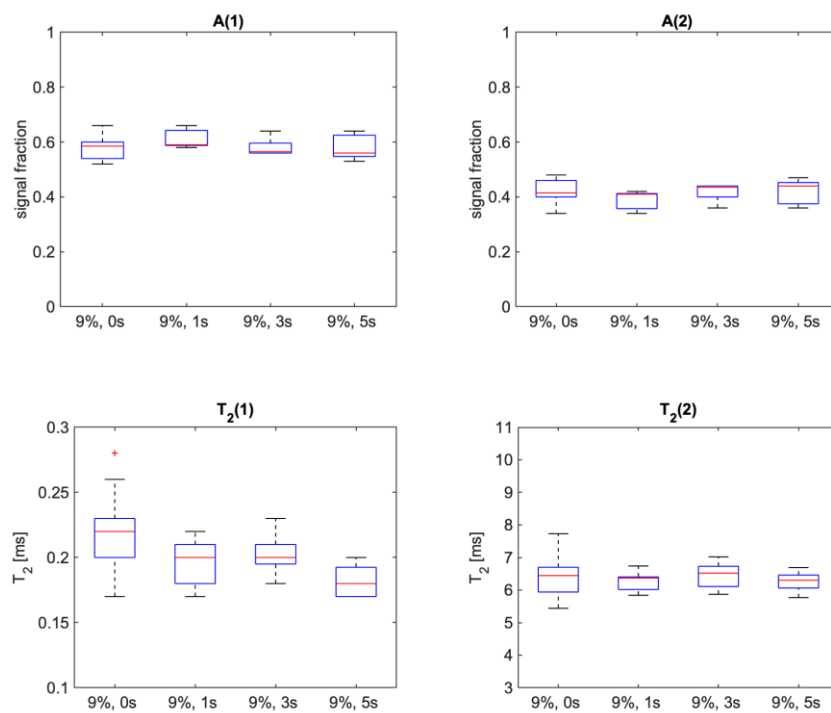


Figure 20: Normalized signal amplitudes (arbitrary units) and T_2 relaxation times (ms) for ABS samples with 9% $Mg(OH)_2$ by weight after thermal exposure. 19 samples total (10 flame tested, 9 untested).

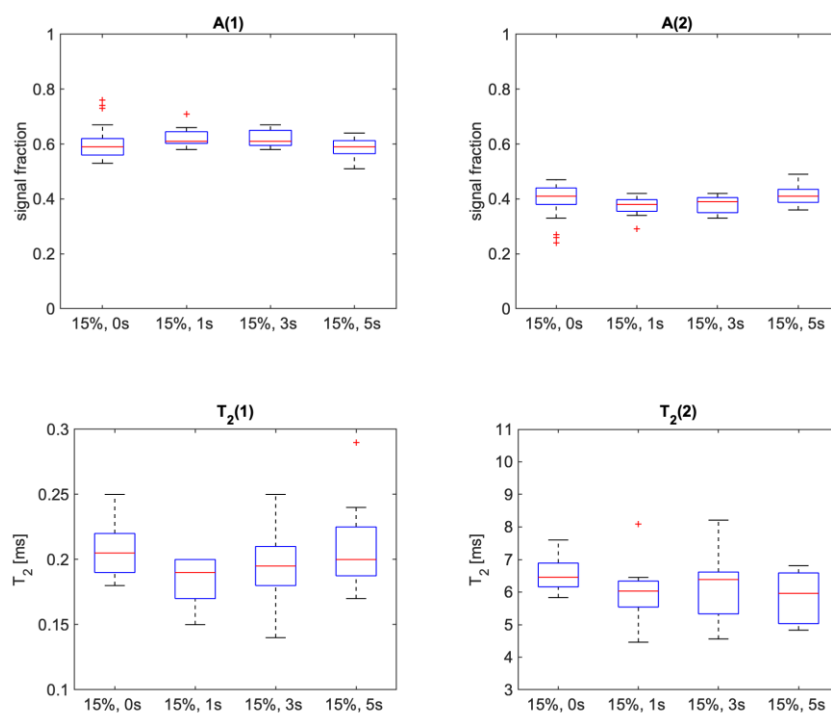


Figure 21: Normalized signal amplitudes (arbitrary units) and T_2 relaxation times (ms) for ABS samples with 15% $\text{Mg}(\text{OH})_2$ by weight after thermal exposure. 20 samples total (10 flame tested, 10 untested).

For the samples with T_2 relaxation times that were responsive to thermal exposure, the smaller T_2 component was the only one that showed change. The larger T_2 component remained consistent, regardless of thermal exposure. While it is unknown what kinds of molecular motion the two T_2 components characterize in the ABS samples, most likely the smaller T_2 component describes the intermolecular motion in the network and the larger T_2 component describes the intramolecular motion in the network.

Thermally degraded ABS is brittle and rigid. This means that more ABS strands in the network have annealed, changing the intermolecular motion in the network. As more strands anneal in the network, the amount of residual dipolar coupling in the sample increases. Increased

residual dipolar coupling in the sample corresponds to faster spin decoherence in a sample. Faster spin decoherence in a sample corresponds to smaller T_2 relaxation values.

Most likely, the intramolecular motion of the ABS polymer strands remained consistent, regardless of thermal exposure, because there was not enough thermal energy present to alter individual strands to the point where change would be detectable with single-sided NMR.

6. Conclusions

Single-sided NMR can be used to characterize the physical properties of ABS, both with and without the presence of $\text{Mg}(\text{OH})_2$ in the polymer network, as seen in the consistent T_2 relaxation times for all unheated ABS and $\text{Mg}(\text{OH})_2$ samples. Single-sided NMR can also be used to characterize changes in the ABS polymer network before and after heat exposure, in addition to the protective effects $\text{Mg}(\text{OH})_2$ has as a flame-resistant additive, as seen in the changes reflected in the T_2 relaxation times.

Future studies should include a more in-depth analysis of the ABS polymer network and its thermal decomposition in order to better contextualize the types of molecular motion that are observed with the two unique T_2 relaxation times present in all ABS samples. This type of study could also be supplemented with data from other analytical techniques such as thermogravimetric analysis (TGA), thermogravimetric analysis-mass spectrometry (TGA-MS), and Fourier-transform infrared spectroscopy (FTIR). It may also be interesting to study the effects of sample thickness on the flame-resistance of thermoplastics, to better characterize the flame-resistance that is achieved from making the thermoplastic shells of fire helmets thicker. Also, single-sided NMR can be used to study solvent effects, UV degradation, and other stressors on the physical properties of thermoplastics, to better characterize and understand the material lifespans of thermoplastics.

Appendix A: Tables

Sample	Length of thermal exposure (s)	Caught fire (Y/N)	Time until flame self-extinguished (s)
Tile 1	1	N	-
Tile 2	1	N	-
Tile 3	1	N	-
Tile 4	3	Y	8
Tile 5	3	Y	19
Tile 6	3	Y	8
Tile 7	3	Y	12
Tile 8	5	Y	3
Tile 9	5	Y	9
Tile 10	5	Y	4

Table 1: Flame test data for 3D printed ABS filament samples.

Sample	Length of thermal exposure (s)	Caught fire (Y/N)	Time until flame self-extinguished (s)
Cast 1	1	N	-
Cast 2	1	N	-
Cast 3	1	N	-
Cast 4	3	Y	157
Cast 5	3	Y	126
Cast 6	3	Y	187
Cast 7	3	Y	7
Cast 8	5	Y	7
Cast 9	5	Y	116
Cast 10	5	Y	4

Table 2: Flame test data for ABS samples cast from acetone.

Sample	Length of thermal exposure (s)	Caught fire (Y/N)	Time until flame self-extinguished (s)
ABS + 3%, 1	1	N	-
ABS + 3%, 2	1	N	-
ABS + 3%, 3	1	N	-
ABS + 3%, 4	3	N	-
ABS + 3%, 5	3	N	-
ABS + 3%, 6	3	N	-
ABS + 3%, 7	3	N	-
ABS + 3%, 8	5	N	-
ABS + 3%, 9	5	Y	82
ABS + 3%, 10	5	Y	70

Table 3: Flame test data for ABS samples with 3% Mg(OH)₂ by weight.

Sample	Length of thermal exposure (s)	Caught fire (Y/N)	Time until flame self-extinguished (s)
ABS + 9%, 1	1	Y	2
ABS + 9%, 2	1	N	-
ABS + 9%, 3	1	N	-
ABS + 9%, 4	3	Y	4
ABS + 9%, 5	3	Y	3
ABS + 9%, 6	3	N	-
ABS + 9%, 7	3	N	-
ABS + 9%, 8	5	Y	88
ABS + 9%, 9	5	Y	19
ABS + 9%, 10	5	Y	166

Table 4: Flame test data for ABS samples with 9% Mg(OH)₂ by weight.

Sample	Length of thermal exposure (s)	Caught fire (Y/N)	Time until flame self-extinguished (s)
ABS + 15%, 1	1	N	-
ABS + 15%, 2	1	N	-
ABS + 15%, 3	1	N	-
ABS + 15%, 4	3	N	-
ABS + 15%, 5	3	Y	107
ABS + 15%, 6	3	N	-
ABS + 15%, 7	3	N	-
ABS + 15%, 8	5	Y	86
ABS + 15%, 9	5	N	-
ABS + 15%, 10	5	Y	2

Table 5: Flame test data for ABS samples with 15% Mg(OH)₂ by weight.

Sample	Median $T_2(1)$ (ms)	Median $T_2(2)$ (ms)	$ \Delta T_2(1) $ (after flame testing - before flame testing) (ms)	$ \Delta T_2(2) $ (after flame testing - before flame testing) (ms)
Tile, before	0.17	7.13	-	-
Tile, 1 second	0.17	8.04	0	0.91
Tile, 3 seconds	0.17	6.66	0	0.47
Tile, 5 seconds	0.18	6.84	0.01	0.29
Cast, before	0.24	6.56	-	-
Cast, 1 second	0.20	6.24	0.04	0.32
Cast, 3 seconds	0.18	6.19	0.06	0.37
Cast, 5 seconds	0.18	6.31	0.06	0.25
3%, before	0.23	7.04	-	-
3%, 1 second	0.20	6.44	0.03	0.60
3%, 3 seconds	0.18	6.51	0.05	0.53
3%, 5 seconds	0.19	6.04	0.04	0.40
9%, before	0.22	6.45	-	-
9%, 1 second	0.20	6.37	0.02	0.08
9%, 3 seconds	0.20	6.52	0.02	0.07
9%, 5 seconds	0.18	6.30	0.04	0.15
15%, before	0.21	6.46	-	-
15%, 1 second	0.19	6.03	0.02	0.43
15%, 3 seconds	0.20	6.39	0.01	0.07
15%, 5 seconds	0.20	5.96	0.01	0.50

Table 6: Median T_2 values of all ABS samples and the absolute value of the differences between median T_2 values before and after flame testing.

Appendix B: Experimentation

CPMG (Kea2 Spectrometer):

B_1 Frequency (MHz)	19.3
90° Pulse Amplitude (dB)	-10
180° Pulse Amplitude (dB)	-4
Pulse Length (μ s)	2.75
Repetition Time (ms)	1000
Number of Scans	512
Number of Echoes	512
Number of Complex Points	16
Dwell Time (μ s)	0.5
Echo Time (μ s)	40
T_1 Relaxation (ms)	40 \pm 2

Debugger Script:

```
procedure (CPMGBD)

# Cache macros
cd("$appdir$\Macros\Kea-NMR")
cachemacro("CPMG.mac", "local")
cd("$appdir$\Macros\Kea-Core")
cachemacro("keaCtrl.mac", "local")
cachemacro("keaRun.mac", "local")
cachemacro("keaPlot.mac", "local")
cachemacro("keaFiles.mac", "local")
cd("$appdir$\Macros\NMR-MOUSE")
cachemacro("Service2.mac", "local")
cacheproc("true")

# Set up gui par

guipar = ["90Amplitude = -10",
          "180Amplitude = -4",
          "accumulate = \"yes\"",
          "acqTime = 0.008",
          "alpha = 1.5e8",
          "autoPhase = \"yes\"",
          "b1Freq = 19.3",
          "bandwidth = 2000",
          "dataDirectory = \"Z:\Data\AST\ABS\"",
          "dummies = 0",
          "dummyEchoes = 0",
          "dwellTime = 0.5",
          "echoShift = 0",
          "echoTime = 40",
          "expName = \"Sample187_Mar30_Flame_5sec\"",
          "expNr = 0",
          "filter = \"no\"",
          "filterType = \"sinebellsquared\"",
          "fitType = \"exp\"",
          "flatFilter = \"no\"",
          "incExpNr = \"yes\"",
          "normalize = \"yes\"",
          "nrEchoes = 512",
          "nrPnts = 16",
          "nrScans = 512",
          "pulseLength = 2.75",
          "repTime = 1000",
          "rxGain = 31",
          "rxPhase = 247",
          "saveData = \"true\"",
          "sumEchoes = \"no\"",
          "timeMag = \"no\"",
          "usePhaseCycle = \"yes\"",
          "x_maximum = 100",
          "x_minimum = 0.2"]

# Run the macro via the backdoor
```

```
for(t = 1 to 3)
  guipar = setlistvalue(guiapar,"expNr","\$t\$")
  CPMG:backdoor(guiapar)
  pause(3)
next(t)

endproc()
```

Appendix C: Data Processing

MATLAB Processing Script:

quickKeaT2.m

```
clear
clc
close all

filename = 'data.2d';
filedir = 'Z:\Data\AST\ABS\Sample187_Mar30_Flame_5sec\3\';
nExp = 2;

omitEchoes = 0; %front-end echoes to omit
% END USER-DEFINED PARAMETERS

fileloc = strcat(filedir,filename);
parloc = strcat(filedir,'acqu.par');

[ap,spec] = readKea4d(fileloc);
tEcho = readpar_Kea(parloc,'echoTime'); %s
nEchoes = ap.yDim;
nPts = ap.xDim;
acqTime = readpar_Kea(parloc,'acqTime')*1e-3; %1e-3 does conversion to s

nPtsBlank = 0; %don't touch

% nExp = 1; %1 for mono, 2 for bi

echoVector = (tEcho:tEcho:nEchoes*tEcho)*1e-6;

data = reshape(spec,nPts,nEchoes);
data = data(1:(nPts-nPtsBlank),:);
data = autophase(data',1);

%%
dataInt = sum(data',1);

dataIntRe = real(dataInt);
dataIntIm = imag(dataInt);

dataOut = dataIntRe'./dataIntRe(1);
echoOut = echoVector';

if nExp == 1
    guess = [1 15e-6];% 0.6 6e-03];
```

```

    [beta,R,J,CovB] = nlinfit(echoVector,dataIntRe./max(dataIntRe),
@t2monofit_simple, guess);
    beta_err = sqrt(diag(CovB));
    ypred = t2monofit_simple(beta,echoVector);

    sprintf('T2 = %f ± %f [us]',1e6*beta(2), 1e6*beta_err(2))
    sprintf('A = %f ± %f [arb]',beta(1), beta_err(1))

    fileID = fopen(strcat(filedir,'T2fit.txt'),'w');
    fprintf(fileID,'Monoexponential Fit\nT2 = %.2f ± %.1g ms\n A = %.2f
± %.1g [arb]',1000*beta(2), 1000*beta_err(2),beta(1), beta_err(1));
    fprintf(fileID,'\ntE = %i us',tEcho);
    fclose(fileID);

elseif nExp == 2
    guess = [0.5 0.23e-3 10e-3 0.03];
    [beta,R,J,CovB] = nlinfit(echoVector,dataIntRe./max(dataIntRe),
@t2bifit_ampSumFixed_offset, guess);
    beta_err = sqrt(diag(CovB));
    ypred = t2bifit_ampSumFixed_offset(beta,echoVector);

    sprintf('A1 = %.2f ± %.1g; A2 = %.2f ± %.1g [arb]',beta(1),
beta_err(1), 1-beta(1), beta_err(1))
    sprintf('T21 = %.2f ± %.1g; T22 = %.2f ± %.1g [ms]',1000*beta(2),
1000*beta_err(2), 1000*beta(3), 1000*beta_err(3))

    fileID = fopen(strcat(filedir,'T2fit.txt'),'w');
    fprintf(fileID,'Biexponential Fit\n');
    fprintf(fileID,'T2(1) = %.2f ± %.1g [ms]\n',1000*beta(2),
1000*beta_err(2));
    fprintf(fileID,' A(1) = %.2f ± %.1g [arb]\n',beta(1), beta_err(1));
    fprintf(fileID,'T2(2) = %.2f ± %.1g [ms]\n',1000*beta(3),
1000*beta_err(3));
    fprintf(fileID,' A(2) = %.2f ± %.1g [arb]\n',1-beta(1), beta_err(1));
    fprintf(fileID,'\ntE = %i us',tEcho);
    fclose(fileID);
elseif nExp == 3
    guess = [0.4 0.1 0.6 0.07 .004 .0022 0];
    [beta,~,~,CovB] = nlinfit(echoVector,dataIntRe./max(dataIntRe),
@t2trifit_y0, guess);
    beta_err = sqrt(diag(CovB));
    ypred = t2trifit_y0(beta,echoVector);
    output = [beta(1:3)'. /sum(beta(1:3)); beta(4:numel(guess))'];
beta_err(1:3) ./sum(beta(1:3)); beta_err(4:numel(guess))];
    output = reshape(output,numel(guess),2);
    output(4:6,:) = output(4:6,:)*1000;
    output(:,3) = output(:,2) ./output(:,1);

```

```

fileID = fopen(strcat(filedir, 'T2fit.txt'), 'w');
fprintf(fileID, 'Triexponential Fit\n');
fprintf(fileID, 'T2(1) = %.2f ± %.1g [ms]\n', output(4,1), output(4,2));
fprintf(fileID, ' A(1) = %.2f ± %.1g [arb]\n', output(1,1), output(1,2));
fprintf(fileID, 'T2(2) = %.2f ± %.1g [ms]\n', output(5,1), output(5,2));
fprintf(fileID, ' A(2) = %.2f ± %.1g [arb]\n', output(2,1), output(2,2));
fprintf(fileID, 'T2(3) = %.2f ± %.1g [ms]\n', output(6,1), output(6,2));
fprintf(fileID, ' A(3) = %.2f ± %.1g [arb]\n', output(3,1), output(3,2));
fprintf(fileID, '\ntE = %i us', tEcho);
fclose(fileID);

end

close all
hh = figure(2);
set(gcf, 'Position', [48 80 910 580])
hold on
plot(1000*echoVector, dataIntRe./max(dataIntRe));
plot(1000*echoVector, dataIntIm./max(dataIntRe));
plot(1000*echoVector, ypred, '-k');
xlabel('time [ms]');
ylabel('intensity');
xlim([0 1000*max(echoVector)])
set(gca, 'FontSize', 18, 'linewidth', 2);
title({'CPMG', strcat(filedir, filename)}, 'Interpreter', 'none')
legend('Real', 'Imag', 'Fit')
legend('boxoff')
pubgraph(hh, 14, 1, 'w', 'Arial');
print(strcat(filedir, filename, '.jpg'), '-djpeg');

```

Appendix D: Abbreviations

ABS	Acrylonitrile butadiene styrene
CPMG	Carr-Purcell-Meiboom-Gill Sequence
Mg(OH) ₂	Magnesium hydroxide
NFPA	National Fire Protection Association
NMR	Nuclear magnetic resonance (spectroscopy)
PPE	Personal protective equipment

Bibliography:

- [1] LaTourette, T.; Peterson, D. J.; Bartis, J. T.; Jackson, B. A.; Houser, A. Protecting Firefighters. In *Protecting Emergency Responders, Volume 2*; RAND Corporation: Santa Monica, 2003; pp 25-42.
- [2] Calvano, N. J.; *Considerations in Establishing Performance Criteria for Structural Firefighters' Helmets*; NSBIR 77-1251; U.S. Department of Commerce National Bureau of Standards: Washington, D.C., 1977.
- [3] MSA; *MSA Cairns Fire Helmet Product Specification*; MSA 3600-74; MSA, 2015.
- [4] Lee, J. Y.; Park, J.; Park, H.; Coca, A.; Kim, J. H.; Taylor, N. A.; Son, S. Y.; Tochiara, Y. What do firefighters desire from the next generation of personal protective equipment? Outcomes from an international survey. *Ind. Health*. **2015**, 53(5), 434-444.
- [5] NFPA. NFPA 1851: Standard on Selection, Care, and Maintenance of Protective Ensembles for Structural Fire Fighting and Proximity Fire Fighting. In *NFPA National Fire Codes Online*; NFPA: Quincy, 2014.
- [6] NFPA Standards Council. In *National Fire Protection Association Annual 2013 Association Technical Meeting*, Chicago, IL, June 12, 2013; National Fire Protection Association: Quincy, MA, 2013.
- [7] NFPA. NFPA: 1971: Standard on Protective Ensembles for Structural Fire Fighting and Proximity Fire Fighting. In *NFPA National Fire Codes Online*; NFPA: Quincy, 2018.
- [8] LaTourette, T.; Peterson, D. J.; Bartis, J. T.; Jackson, B. A.; Houser, A. Procurement and Logistics. In *Protecting Emergency Responders, Volume 2*; RAND Corporation: Santa Monica, 2003; pp 89-102.
- [9] Kiliaris, P.; Papaspyrides, C. D. Chapter 1 - Polymers on Fire. In *Polymer Green Flame Retardants*, 1st ed.; Elsevier: Amsterdam, 2014; pp 1-43.
- [10] Berardi, U.; Dembsey, N. Thermal and Fire Characteristics of FRP Composites for Architectural Application. *Polymers*. **2015**, 7(11), 2276-2289.
- [11] Bart, J. C. J. Polymer/additive analysis by flash pyrolysis techniques. *J. Anal. Appl. Pyrolysis*. **2001**, 58-59, 3-28.
- [12] Casanova, F.; Perlo, J.; Blümich, B. *Single-Sided NMR*; Springer: Heidelberg, 2011.
- [13] Brass, M.; Morin, F.; Meldrum, T. Spatially Resolved Measurements of Crosslinking in UV-Curable Coatings using Single-Sided NMR. *Magnetochemistry*. **2018**, 4(1), 8.

[14] Beard, A., Reilley, T. Additives used in Flame Retardant Polymer Formulations: Current Practice & Trends, 2009.

[15] Wang, S.; Hu, Y.; Zong, R.; Tang, Y.; Chen, Z.; Fan, W. Preparation and characteristic of flame retardant ABS/montmorillonite nanocomposite. *Appl. Clay Sci.* **2004**, 25(1), 49-55.

[16] Ma, H.; Tong, L.; Xu, Z.; Fang, Z.; Jin, Y.; Lu, F. A novel intumescent flame retardant: Synthesis and application in ABS copolymer, *Polym. Degrad. Stab.* **2007**, 92(4), 720-726.

[17] James, T. Fundamentals of NMR. In *Biophysics Textbook Online*; Biophysical Society: San Francisco, 1998; pp 1-31.